Synthesis and thermoluminescence properties of $MgAl_2O_4$:Ca laser-sintered ceramics

*N. M. Trindade[1,2], E. P. Silva[3], M. C. S. Nunes[1], J. M. Munoz[1], J. C. A. Santos[4], E. M. Yoshimura[2], R. S. Silva[3]

[1] Department of Physics, Federal Institute of Education, Science and Technology of São Paulo, 01109-010, São Paulo, SP, Brazil.

[2] Institute of Physics, University of São Paulo, 05508-090, São Paulo, SP, Brazil.

[3] Department of Physics, Federal University of Sergipe, 49100-000 São Cristóvão, SE, Brazil

[4] Center of Exact and Technological Science, Federal University of Recôncavo of Bahia, Cruz das Almas, 44380-000, BA, Brazil

*email: ntrindade@ifsp.edu.br

ABSTRACT

Ceramic materials are low cost and have a good thermal and mechanic resistance which are suitable characteristics for a good dosimeter. A new Ca-doped $MgAl_2O_4$ ceramic material was produced by the first time by the laser sintering method. Thermoluminescence (TL) properties as a function of the exposure to ionizing radiation were investigated. X-ray diffraction of the sintered samples showed single crystalline phase corresponding to the cubic spinel structure. SEM images reveal the microstructure with homogenous and faceted grains and low porosity. TL readouts were performed with a linear heating rate were performed after irradiation with beta particles (doses ranging from 0.02 to 5 Gy). The TL glow-curve shows a single and wide peak centered at about 170^{o}C with a linear dose response, good repeatability (~1%) and immediate fading that stabilizes after ~16h with 80% of the initial intensity. The lowest detectable dose (*LDD*) was also evaluated at ~ 20 μGy. By applying the T_m-T_{stop} method to analyze the glow curve, it was found a behavior characteristic of closely overlapping or a quasi-continuum of peaks. Initial Rise, peak shape of the TL glow curve, the TL glow curve area, and glow curve fitting methods were used to obtain the kinetic parameters of the glow peak. In general, the TL results suggest that this material might be used in dosimetric applications considering the studied dose range.

Keywords: $MgAl_2O_4$:Ca, thermoluminescence, dosimetry, laser sintering.

1. INTRODUCTION

Dosimetric materials are used for the determination of the absorbed dose received from ionizing radiation in the environment as well as in medical and technological activities [1,2]. In addition, synthetic dosimeters have the advantage of controlled synthesis and precise chemical composition thus presenting good inter and intra-batches reproducibility. Thermoluminescence (TL) and optically stimulated luminescence (OSL) have been used extensively to evaluate materials for dosimetry application [3–12].

TL is the light emitted by some crystals when heated, being a thermally stimulated emission of the energy that was previously stored in the material during irradiation [5]. TL materials are usually ionic crystals, in which the valence band is filled with electrons and the conduction band is empty, and between these bands there is an energy gap. Defects in the material can generate energy levels within the gap, which act as traps for charged carriers (electrons or holes). Exposure of material to ionizing radiation distributes charge carriers to the trap levels, while heating leads to the release of the charge carriers from traps [13]. Recombination of charges at luminescent centers produces a measurable light emission, with intensity commensurate with the number of trapped charges. The resulting TL signal usually is proportional to the absorbed dose in a large range of doses [5,14].

The material under consideration in this paper is magnesium aluminum spinel ($MgAl_2O_4$) that is an insulating oxide with important chemical, thermal, mechanical, dielectric and optical properties [15–17]. $MgAl_2O_4$ spinel presents cubic structure with divalent cations (Mg^{2+}) occupying tetrahedral sites while trivalent cations (Al^{3+}) are in octahedral sites [16]. However, some amount of Al^{3+} ions occupies tetrahedral sites while Mg^{2+} occupies octahedral sites [18]. The presence of a high concentration of intrinsic defects and disorder in $MgAl_2O_4$ samples lead to

the formation of point defects with different charge, so-called antisite defects: $(Al_{Mg}^{3+})^{+}$ and $(Mg_{Al}^{2+})^{-}$ centers [18,19]. Therefore, those locally charged lattice defects may act as electron and hole traps [16,19,20]. In addition, based on Kumamoto's studies [21] on Ca-doped MgO, the great difference between the Ca^{2+} (0.9 Å, coordination number, CN: 6) and Mg^{2+} ion (0.57 Å , CN: 4) ionic radius, could generate additional lattice defects. Within this context, when exposure to ionizing radiation occurs, trapping and detrapping processes related to these defects that can be studied by the TL technique and its dosimetric characteristics can be studied. Several works have shown that the $MgAl_2O_4$ spinel is a great candidate for use as dosimeter [16,22–27]. Interestingly, $MgAl_2O_4$ has chemical stability for various cationic impurities while maintaining optical properties [16,25].

In this research, we have produced Ca doped $MgAl_2O_4$ spinel powders by polymeric precursors method and ceramic bodies using the laser sintering technique. The laser sintering has received considerable attention because of its potential application to obtain dense ceramics oxides with different chemical compositions and properties [28–32]. The great differential of this technique is the use of a CO_2 laser as the main heating source and whose main advantages are: (1) the fast process, few minutes, because the oxides effectively absorb CO_2 laser radiation [33,34]; (2) the inhibition of contaminations as it does not use crucible [34]; (3) the high heating and cooling rates (about 2000 °C/min), that can allow the generation of new defects. As examples of possible defects and related properties: oxygen vacancies in $Bi_4Ge_3O_{12}$ [33,35], Y_2O_3 [36] and $BaTiO_3$:La [28] ceramics, the reduction of Eu^{3+} to Eu^{2+} in luminescence persistent materials even in when sintered in open atmosphere [29,31,32] and modifications on electrical response in $(Cu,Bi)Ca_3Ti_4O_{12}$ [37,38]. In particular, in $Bi_4Ge_3O_{12}$, the laser-sintered ceramic presented higher transparency, lower TL peaks and better scintillators characteristics when compared with the

conventionally sintered ceramics [33,35]. The authors suggest that these responses are due to a lower density of trap centers, related to oxygen or bismuth vacancies, when the samples are laser-sintered in contrast to the prolonged sintering time in electrical furnace. Therefore, besides the sintering, the TL dosimetric and kinetic properties of $MgAl_2O_4$:Ca ceramics are reported here for the first time.

2. MATERIALS AND METHODS

Ca doped $MgAl_2O_4$ powder (1 mol% of Ca) was synthesized by a modified polymeric precursor method using magnesium chloride hexahydrate($Cl_2H_{12}MgO_6$, 99%, Neon), aluminum chloride hexahydrate ($AlCl_3H_{12}O_6$, 99%, Aldrich), calcium carbonate ($CaCO_3$, 99%, Aldrich), citric acid ($C_6H_8O_7$, PA, Synth) and ethylene glycol ($C_2H_6O_2$, PA, Dinâmica) as precursors materials. Magnesium and aluminum citrates were separately prepared using metal precursors mixed with citric acid (CA), previously dissolved in distilled water (0.1 g/ml), at the molar ratio of 1:3 (Metal:CA). Then, ethylene glycol (EG) was added to these solutions, in the mass ratio of 3:2 (CA:EG), in order to promote citrate polymerization by the polyesterification reaction. After, 1 mol% of calcium carbonate was added to the Mg solution. Both solutions were then mixed and heated (under stirring) up to 120 °C until a stable and transparent viscous resin to be obtained. Finally, this resin was thermally treated at 600 °C for 5 h, and the resultant powder was calcined at 1000 °C for 2h. The calcined powders were uniaxially compacted into disks of 4 mm diameter and ~1.0 mm thickness using a pressure of 90 kgf. The sintering was performed using a CO_2 laser (GEM-100L, Coherent) in continuous-wave mode as the unique heating source. In the laser sintering technique, the sample is put on a base composed of the same material to be sintered and the laser beam (diameter of 6.7 ± 0.3 mm) is directed and held at the center of the sample throughout the sintering process. The samples were sintered at a power density of 2.8 ± 0.1

W/mm^2, with a dwell time of 90 s. The entire sintering process lasted approximately 10 min. The whole synthesis and sintering process were conducted in air.

The structural investigation was made by powder X-ray diffraction analysis in a XRD – Rigaku diffractometer RINT 2000/PC, using Cu Kα radiation. The measurements were carried out at room temperature in continuous mode, in the 2θ range between 20° to 80°, in steps of 0.02°. The microstructures of the ceramics were analyzed through scanning electron microscopy (SEM – JEOL – JSM 6510-LV).

TL measurements were carried out using a commercial automated TL/OSL reader made by Risø National Laboratory (model DA-20). TL glow curves were obtained from RT to 400 ºC, no mask. The TL signal was detected with a bialkali photomultiplier tube behind an UV-transmitting glass filter (Hoya U-340, 7.5 mm thick). Irradiation was performed at room temperature using a ^{90}Sr/^{90}Y beta source from the TL reader (dose rate of 10 mGy/s). The analysis of the glow curves and the extraction of the kinetic parameters involved several methods, including T_m-T_{stop}, T_m as a function of irradiation dose (dose range from 20 mGy to 5 Gy), Initial Rise, peak shape of the TL glow curve, the TL glow curve area and glow curve fitting methods.

3. RESULTS AND DISCUSSION

3.1 – Sample production

Fig. 1 presents the XRD patterns of the $MgAl_2O_4$:Ca laser-sintered ceramic. The sample shows single crystalline phase corresponding to the cubic spinel structure (Fd-3m), indexed according to Inorganic Crystal Structure Database - ICSD (PDF 16-7484). In addition, no spurious phase was observed, suggesting that Ca ions have been successfully inserted in $MgAl_2O_4$ structure. The SEM images of the surface and fractured surface cross section of the ceramic are displayed in

Fig. 2. It presents good microstructure with homogeneous and faceted grains with grain size distribution from ~ 3 - 12µm (Fig. 2a). In Fig. 2b it is possible to see the presence of porous in the inter- (larger porous) and intra-grain (smaller porous) regions.

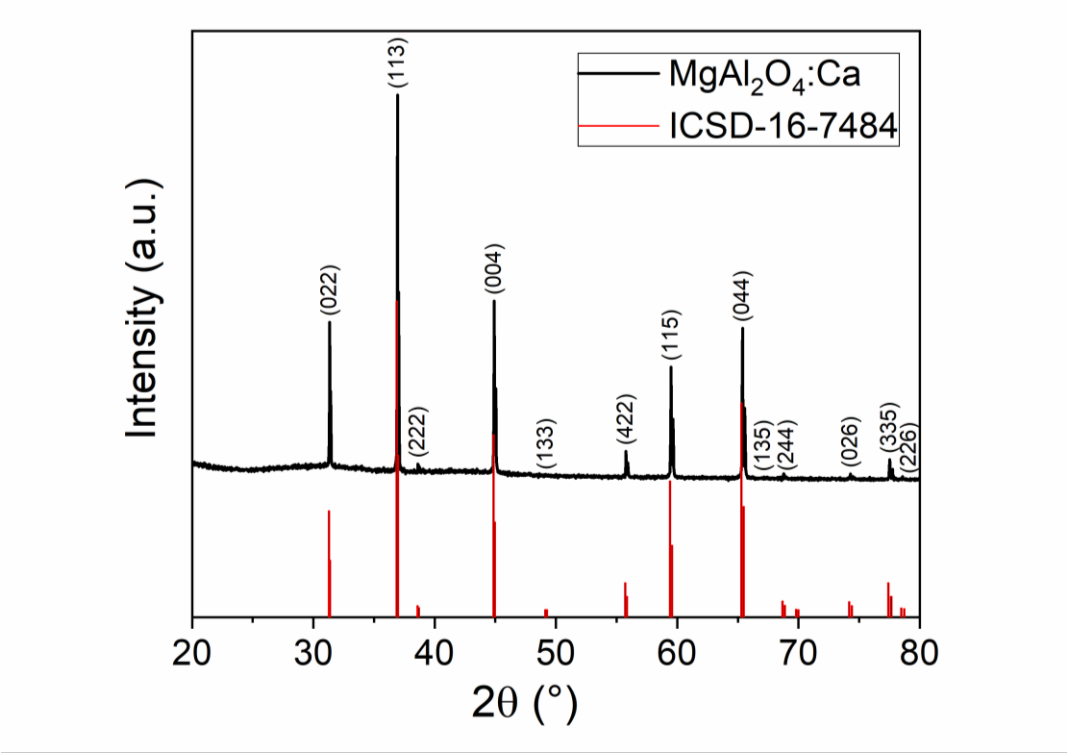

Figure 1: XRD patterns of the $MgAl_2O_4$:Ca laser-sintered ceramic. Reflection peaks were indexed according to the Inorganic Crystal Structure Database (ICSD-16-7484).

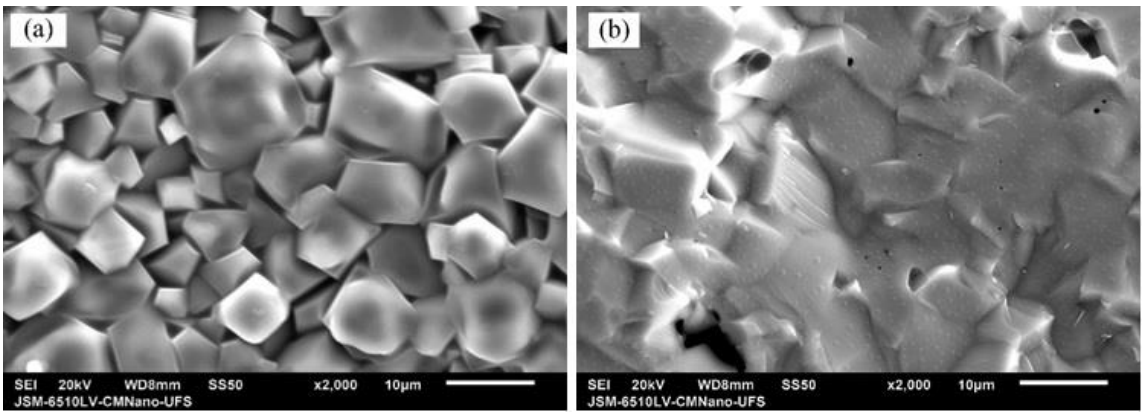

Figure 2: SEM images of the surface (a) and cross-section (b) of the ceramics.

3.2 – TL dosimetric characterization

Fig. 3a shows the TL glow curves of the $MgAl_2O_4$:Ca laser-sintered ceramic measured at 1 °C/s, for various absorbed doses, from 100 mGy to 5 Gy and taken immediately after the exposure. Unlike other studies with $MgAl_2O_4$, only one TL peak is observed in this study. Ibarra and colleagues report 2 TL peaks (350 K and 500 K at 0.17 K/s) in synthetic samples irradiated with X-rays and γ rays [39]. Yoshimura and Yukihara [16] observed 3 peaks in beta irradiated samples - peak I, at 63 °C, a broad peak II, ranging from 200 to 280°C, and a peak III at 450°C (at 1 K/s). According to [16,39], an Al^{3+} ion occupying a Mg site may be related to an electron trap while a Mg^{2+} ion replacing an Al site would be a hole trap. Nevertheless, in this work, the glow curves exhibit a single wide peak ranging from 50 °C to 350 °C, centered at about 170 °C. Probably, due to the incompatibility of ionic radii between Ca^{2+} and Mg^{2+} in the crystal structure of our sample [21], there is an increase in the number of trapping centers, giving rise to the wide peak observed. In Fig. 3b it is possible to see that the total area under the TL glow curve has very good linearity with dose, with a regression coefficient of 0.9999 even considering the linear coefficient as zero. This result suggests that this material might be used in dosimetric applications considering this dose range.

A study of the immediate fading of the TL signal was also conducted. In this experiment, the sample was irradiated and stored in the dark, at room temperature, for various periods before the TL readout. Glow curves for the samples exposed to 100mGy and after 5, 15, 30, 60 and 1000 min storage periods are compared to an immediate readout glow curve in Figure 4a. The normalized area of the peak as a function of the time after irradiation is presented in Fig. 4b.

Although the peak does not shift in temperature, the lower temperature side of the peak fades preferentially with the time of storage at room temperature. This is due to leakage of trapped

charges from shallower traps [40]. The area under the TL glow curve shows a fast-initial fading (15% after 60 min) and after 1000 min it is reduced to about 80% of the initial value.

A cycle of 5 repetitions of irradiation to 100mGy, followed by immediate readout, for the same detector, gave rise to a coefficient of variation (CV = standard deviation/mean value) of the TL peak area better than 1 %, This is a good estimation to the experimental uncertainty that is expected in an application of pellets like this in a dosimetry procedure.

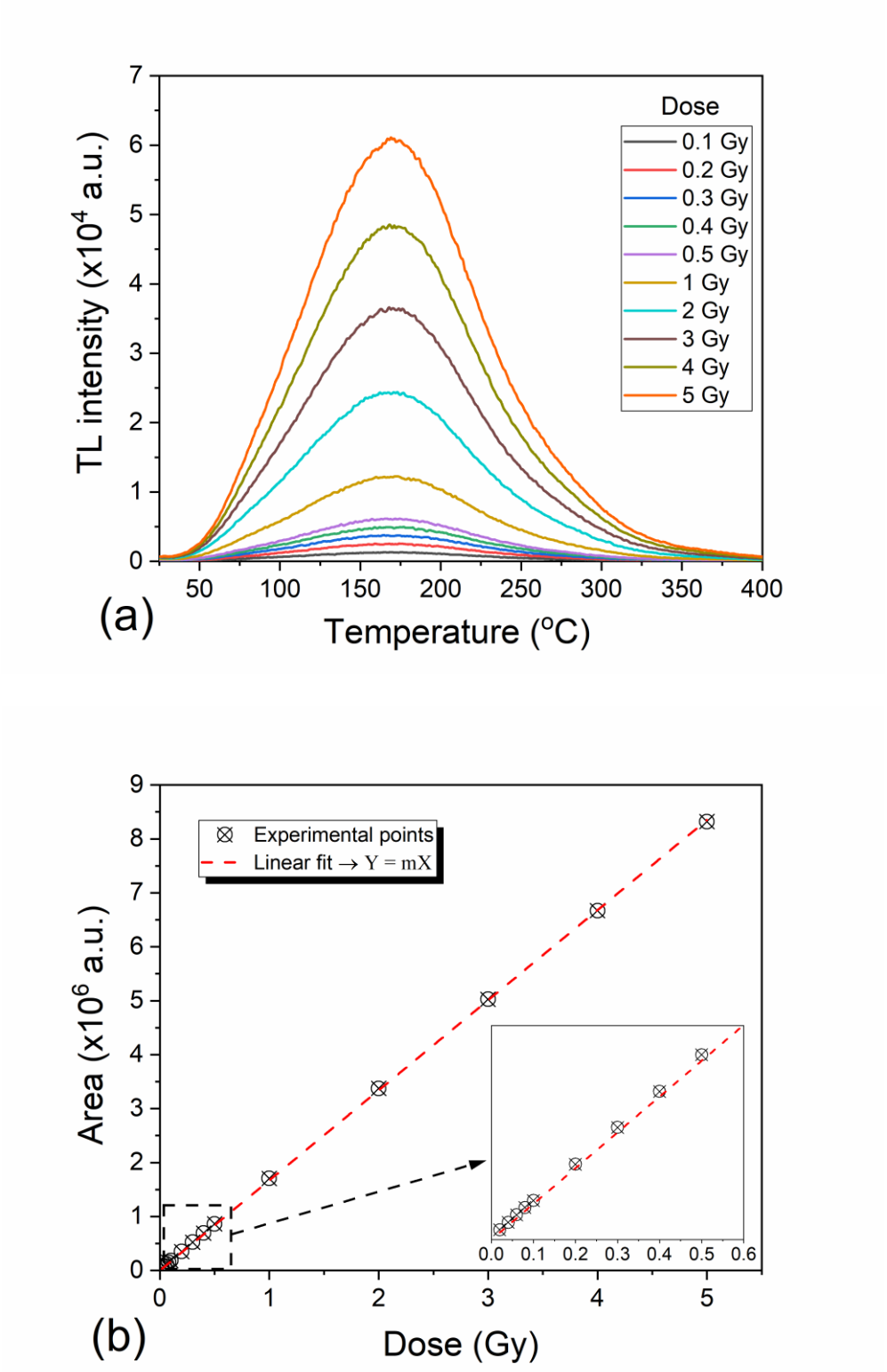

Figure 3: (a) TL glow curves of $MgAl_2O_4$:Ca ceramic for absorbed doses varying from 0.02 to 5 Gy, obtained at a heating rate of 1 °C/s. (b) Integrated intensity is presented as a function of dose, with a linear fitting.

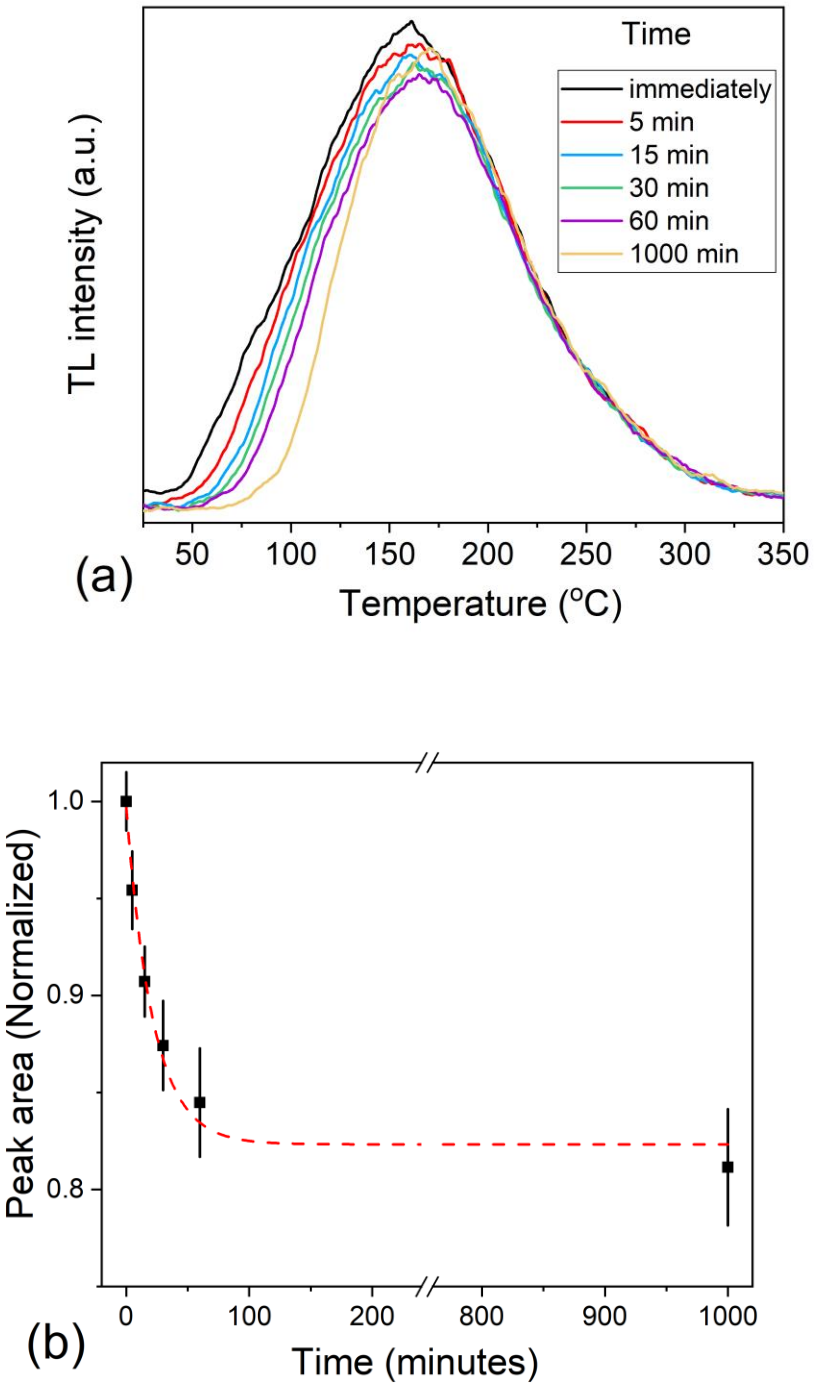

Figure 4: (a) TL glow curves of $MgAl_2O_4$:Ca ceramic for various storage times after beta irradiation to 100 mGy. (b) Normalized TL glow curve area as a function of storage time after beta irradiation to 100 mGy. The line is a guide for the eyes.

3.3 – TL glow curve kinetic study

From the analysis of the individual peaks of the TL glow curve, it is possible to determine the kinetic parameters such as activation energy *E*, the attempt to escape the frequency factor *S* and the kinetic order *b* [41]. The study of the TL kinetics gives us information about the trapping mechanism and defect formation of the studied material.

Firstly, in order to analyze quantitatively the peak shape shown in Fig. 3, the geometric shape factor μ, given by Halperin and Braner [42] was used. The factor has been calculated by the following expression (1) [43]:

$$\mu = \frac{T_2 - T_m}{T_2 - T_1} \qquad (1)$$

where T_m is the temperature at the peak; T_1 and T_2 are the positions of the half-maximum intensity points on the low and high temperature sides of T_m respectively. According to Chen [44], $\mu \cong 0.42$ indicates a first-order peak and $\mu \cong 0.52$ is attributed to a second-order peak. Likewise, second-order kinetic TL peaks are almost symmetric around the luminescence maximum, while first-order kinetic curves are asymmetry [41]. According to this method, the value of $\mu = 0.48 \pm 0.05$ was obtained for our samples (100 mGy dose and a heating rate of 1 ^{o}C/s). This value indicates a general-order peak, corresponding to $b \sim 1.5$ [45,46].

According to the peak shape analyses, the trap activation energy (E_a) can be determined by equation (2).

$$E_\alpha = c_\alpha \left(\frac{kT_m^2}{\alpha}\right) - b_\alpha (2kT_m) \qquad (2)$$

where c_α and b_α are parameters that depend on symmetry factors $\tau = T_m - T_1$, $\delta = T_2 - T_m$ and $\omega = T_2 - T_1$ [41,46], given by equation (3).

$$
\begin{aligned}
c_\tau &= 1.510 + 3.0(\mu - 0.42), \quad & b_\tau &= 1.58 + 4.2(\mu - 0.42) \\
c_\delta &= 0.976 + 7.3(\mu - 0.42), & b_\delta &= 0 \\
c_\omega &= 2.52 + 10.2(\mu - 0.42), & b_\omega &= 1
\end{aligned}
\tag{3}
$$

Based on these equations, the results obtained for activation energy of traps were $E_\tau = (0.31 \pm 0.04)$ eV; $E_\delta = (0.41 \pm 0.04)$ eV and $E_\omega = (0.36 \pm 0.02)$ eV.

To determine the number of peaks, as well as the position of individual peaks present in TL glow curves, the T_m x T_{stop}, method proposed by Mckeever [47] was used. To carry out this characterization, the sample previously irradiated with 100 mGy was heated (q = 1 $^oC/s$) to a T_{stop} temperature, being quickly cooled to room temperature. With this heating, the TL signal below this temperature T_{stop} is cleaned, but the higher temperature signal remains. Then, the sample is reheated to check the remaining TL curve. From this curve, the peak position (T_m) is checked. This process is repeated several times, increasing the T_{stop} temperature in steps of 5 ^oC, between temperatures 60 to 280 ^oC. A graph of peak position in function of the T_{stop} temperature has information of the kinetics of charge de-trapping. Fig. 5 presents the T_m x T_{stop} curve of the sample. According to references [5,47], for a first-order kinetics process, the T_m x T_{stop} curve is characterized by a plateau, meaning that T_m does not change as T_{stop} increases, up to the complete emptying of the trap connected to that particular TL peak. While, for second- and general-order TL peaks, the maximum temperature is a flat line in the beginning but starts increasing as T_{stop} increases, so the T_m x T_{stop} curve is an increasing function. Therefore, according to the T_m x T_{stop} curve (Fig. 5) the TL peak of this sample obeys second or general order kinetics. In fact, the non-ending increase behavior suggests that there is a quasi-continuum of peaks [5,47]. The results found in the literature [39] for transparent single-crystal and polycrystalline samples of $MgAl_2O_4$ irradiated with UV, γ and X-rays concludes, from two TL peaks (~ 75^oC and 225^oC), that these are non-first-order, however, no in-depth kinetic study is presented.

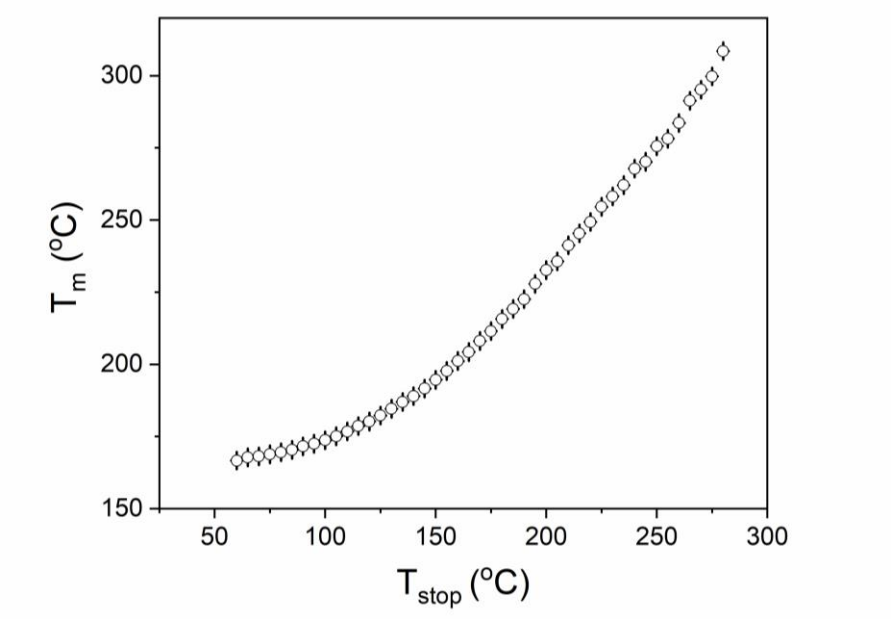

Figure 5: T_m *x* T_{stop} curve of the $MgAl_2O_4$:Ca laser-sintered ceramics with 100 mGy irradiation dose. The measurements were done in steps of 5 °C.

The Initial Rise method proposed by Garlick & Gibson [48] was used to study the activation energy the TL glow curve. For the application this method, it is considered that the concentration of electrons in the traps of the TL process is constant at the low temperature part (the initial rise) of the peak. This way, the initial part of a glow peak (less than 15% of the maximum TL intensity) of the glow peak, is expected to be represented by equation (4) [41]. From the straight line observed in a plot of *ln I* versus *1/kT* the slope is the value of activation energy (*E*). *k* is the Boltzmann constant and the intercept *lnC* is related to the frequency factor (*S*) in a way that depends on the kinetic order.

$$I\,(T) = C\,\exp\left(-\frac{E}{kT}\right) \qquad (4)$$

When the same sample is heated up and cooled down several times, with the maximum temperature of each cycle slightly higher than the preceding one, a series of activation energies can be calculated from the slope of each initial rise curve. This method is often called “fractional

glow curve technique" and was first proposed by Gobrecht and Hofmann [49]. Plotting the energy obtained from each slope as a function of the midpoint temperature of the corresponding initial rise curve reached in that particular cycle [46], it is possible to check three important features [50]: i) the number of the TL peaks in that particular temperature region; ii) the average activation energy of each TL peak; and iii) the distribution of activation energies of charge traps rather than to a single trap energy if there is such a distribution. Sixteen heating and cooling cycles (heating rate of 1°C/s) with 10°C increment in the maximum temperature, from 60 to 210°C were used. This was done here for samples irradiated to 5 Gy (Fig. 6). We observe a continuous rise of the energy when the temperature increases suggesting a distribution of energies for the charge traps, from 0.42 to 0.82 eV, with a mean value of E = (0.70 ± 0.14) eV. The augment of the activation energy with the previous heating temperature corroborates the results of T_m x T_{stop} method, consistent with a quasi-continuum of defects available for the charge carriers.

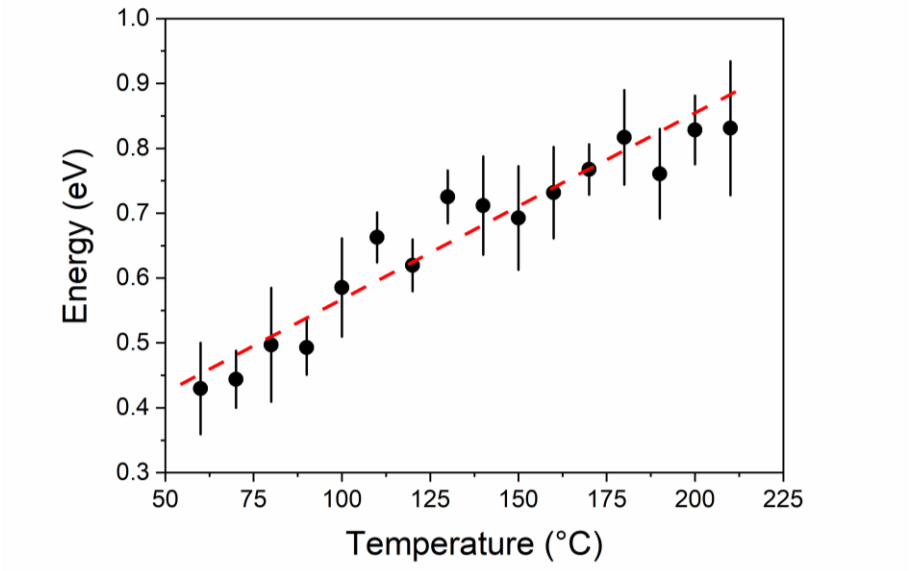

Figure 6: Energy value as a function of the temperature obtained by the Initial Rise method. In this case the samples were 5 Gy irradiated. The red dash line is a straight line in adjusted to indicate a distribution of energies of charge traps.

Other method used to obtain the kinetic parameters associated with TL glow curve is the "area method" or "whole glow peak" [41]. It consists of performing the integral of the TL glow peak from an initial temperature, before the maximum, up to the final temperature at the end of the glow peak. When the kinetic order is unknown, for general order, the following equation (5) can be used:

$$ln\left(\frac{I}{n^b}\right) = ln\left(\frac{S'}{q}\right) - \frac{E}{kT} \quad (5)$$

where I is the intensity of the emitted light at temperature T, n is the area under the glow curve from T to the end of the peak, q is the heating rate, and S', the effective frequency factor, is the relationship between s and the concentration of available electron traps N ($S' = S/N$) [5]. From the straight line observed in a plot of $ln\ (I/n^b)$ versus $1/kT$ the slope gives the value of the activation energy (E). The effective frequency factor can be determined from the line intercept, following equation (6):

$$S' = qe^{intercept} \quad (6)$$

The graph can be plotted with several values of the kinetic order b and the best linear fitting (evaluated by the R^2 coefficient) corresponds to the best value of b. For this method, the glow curve area was determined using the values from 50 to 300 °C. Fig. 7 shows the selected curves for kinetic order values $0 < b < 2.0$. The curve of the best R^2 was that corresponding to $b = 1.5$, $E = (0.343 \pm 0.002)$ eV and $S' = (5.1 \pm 0.3) \times 10^{-2}$.

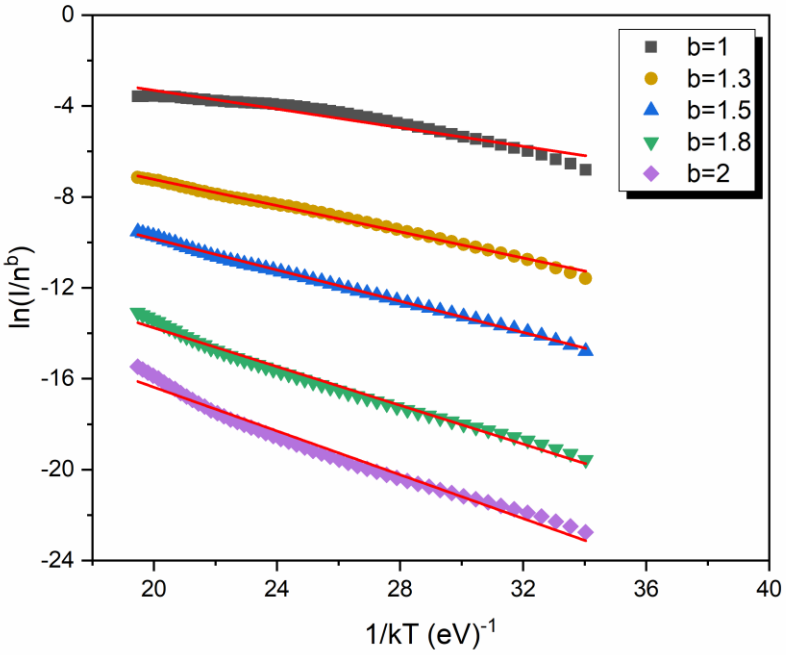

Figure 7: ln (I/n^b) vs *1/kT* from TL glow peak for $MgAl_2O_4$:Ca laser-sintered ceramic for several values of kinetic order *b*, with corresponding linear fits. In this case the sample was 100 mGy irradiated.

The TL glow curve deconvolution ("tgcd") in R-*software* package [51] was the last method used. The package performs the determination of kinetic parameters by different methods. For general-order kinetics, the equations are based on previous studies [51–54]. The quality of these fittings is verified by the figure of merit (FOM) parameter [55]. The software realizes the fitting of the TL glow curves using a Levenberg-Marquardt algorithm modified to support constraints and fixes of parameters. The first function used in this work was developed in Ref. [53], and is given by equation (7).

$$I(T) = I_m b^{b/b-1} \upsilon \times \left[(b-1)\left(1 - \frac{2\mathrm{kT}}{\mathrm{E}}\right)\frac{T^2}{T_m^2}\upsilon + Z_m \right]^{-\frac{b}{b-1}} \quad (7)$$

where $\upsilon = exp\left(\frac{E}{kT}\frac{T-T_m}{T_m}\right)$ and $Z_m = 1 + \frac{2kT_m(b-1)}{E}$

The frequency factor is determined based on the condition for maximum intensity [53,56] given by equation (8).

$$S = \frac{qE}{kT_m^2}\frac{1}{Z_m}exp\left(\frac{E}{kT_m}\right) \quad (8)$$

Fig. 8. illustrates an adjusted TL glow curve performed in "tgcd" package for $MgAl_2O_4$:Ca, obtained after 100 mGy of beta irradiation dose and q of 1°C/s. The TL parameters of glow peak determined by "tgcd" are listed in Table 1. The result indicates this material follows general-order kinetics (b = 1.6), E = 0.33 eV and S´ = 1.2 x 10^2. The analysis showed FOM value is found to be < 4 % for the fitting, which is a sign of agreement between the experimental data and fitting curves.

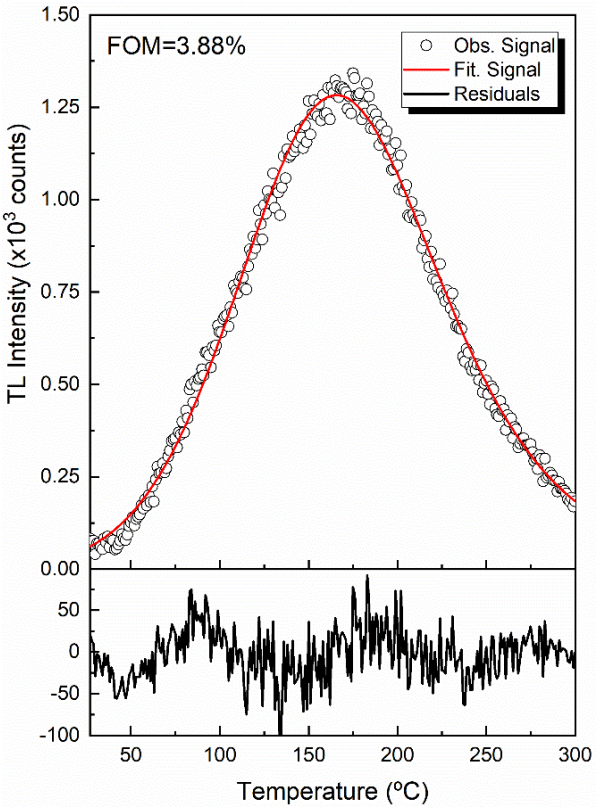

Figure 8: TL glow curve of $MgAl_2O_4$:Ca sample irradiated with 100mGy. The glow curve fitted with general-order peak.

Finally, we summarize in Table 1 the results of the various methods used to analyze the experimental data. In all cases, a general-order kinetics was indicated. To best of our knowledge, this is the first time that a kinetic study is done for $MgAl_2O_4$:Ca system.

Table 1: Summary of the results of energy (*E*), effective frequency factor *S´* and kinetic order *b* of $MgAl_2O_4$:Ca for various analysis methods for general-order data.

Method	*E* (eV)	*S´*	*b*
Chen´s τ	0.31 ± 0.04		
Chen´s δ	0.41 ± 0.04		1.5
Chen´s ω	0.36 ± 0.02		
Initial Rise	0.42 to 0.82		
Whole Glow Peak	0.343 ± 0.002	$(5.1 \pm 0.3) \times 10^{-2}$	1.5
"tgcd"	0.33	1.20×10^{2}	1.6

3.4 – Lowest detectable dose

An important parameter for a dosimetric applications is the lowest detectable dose (*LDD*). Usually, the *LDD* is calculated by equation (9) [57,58]:

$$LDD = (\bar{B} + 3\sigma_{\bar{B}}) \cdot f_c \qquad (9)$$

where $\bar{B}$ is the mean TL response background signal from the non-irradiated samples, $\sigma_{\bar{B}}$ is the standard deviation of measurement of the mean background of non-irradiated samples and f_c is the calibration factor that is obtained from the inverse of the slope of the TL response as a function of absorbed dose (Fig. 3b). For the samples used in this work, *LDD* of 18 μGy was obtained. This value is suggestive of applications in various fields of dosimetry, like personal and medical dosimetry.

CONCLUSIONS

In this work, Ca doped $MgAl_2O_4$ spinel ceramics were produced by laser sintering technique for the first time. According to XRD analysis the $MgAl_2O_4$ matrix has cubic spinel structure without the formation of spurious phases. SEM images confirmed the good microstructure of the laser-sintered ceramics that present homogeneous grains in the micrometer scale. The TL results showed important characteristics for dosimetry, including that there is a high intensity TL peak (~ 170^{o}C at 1^{o}C/s), with a linear dose response for beta irradiation and ~1% of uncertainty for each dosimeter, *LDD* of ~20 μGy. The fast-initial fading (20% reduction after ~ 16 h.) indicates that some adjustments in material defect structure may be done to improve its performance. Finally, the kinetic study showed that the wide TL glow curve can be interpreted as composed by a quasi-continuum of closely overlapping peaks, or by one peak with kinetic order ~1.5. Either hypotheses agree with the average activation energy of ~ 0.4 eV.

ACKNOWLEDGMENTS

N. M. Trindade (#2019/05915-3), M. C. S. Nunes (#2018/16894-4) and J. M. Munoz (#2019/22375-2) are grateful to São Paulo Research Foundation (FAPESP). R. S. Silva, E. P. Silva and J. C. A. Santos are grateful to National Council for Scientific and Technological Development (CNPq) – Brazil, grant #409017/2016-7. E. M. Yoshimura is grateful to FAPESP, grant #2018/05982-0 and CNPq, grant #306843/2018-8.

REFERENCES

[1] E.G. Yukihara, S.W.S. Mckeever, Optically Stimulated Luminescence: Fundamentals and Applications, UK: John Wiley and Sons, West Sussex, 2011.

[2] S.S. Lalic, D.N. Souza, O. Baffa, F. D´Errico, New dosimetric materials for applications in medical physics, Rev. Bras. Física Médica. 13 (2019) 10. https://doi.org/10.29384/rbfm.2019.v13.n1.p24-33.

[3] N.K. Umisedo, E. Okuno, F. Cancio, E.M. Yoshimura, R. Künzel, Development of a mechanically resistant fluorite-based pellet to be used in personal dosimetry, Radiat. Meas. 134 (2020) 106330. https://doi.org/10.1016/j.radmeas.2020.106330.

[4] E.G. Yukihara, S.W.S. McKeever, M.S. Akselrod, State of art: Optically stimulated luminescence dosimetry – Frontiers of future research, Radiat. Meas. 71 (2014) 15–24. https://doi.org/https://doi.org/10.1016/j.radmeas.2014.03.023.

[5] S.W.S. McKeever, Thermoluminescence of Solids, Cambridge University Press, Cambridge, 1985. https://doi.org/10.1017/cbo9780511564994.

[6] L. Botter-Jensen, S.W.S. McKeever, A.G. Wintle, Optically Stimulated Luminescence Dosimetry, Elsevier Science, Amsterdam, 2003. https://doi.org/10.1016/B978-0-444-50684-9.X5077-6.

[7] N.M. Trindade, L.G. Jacobsohn, E.M. Yoshimura, Correlation between thermoluminescence and optically stimulated luminescence of α-Al_2O_3:C,Mg, J. Lumin. 206 (2019) 298–301. https://doi.org/https://doi.org/10.1016/j.jlumin.2018.10.084.

[8] S.L. Dardengo, M.C.S. Nunes, C. Ulsen, E.M. Yoshimura, N.M. Trindade, Investigação da termoluminescência de alexandrita ($BeAl_2O_4$: Cr^{3+}), Brazilian J. Radiat. Sci. in press (n.d.).

[9] N.M. Trindade, M.G. Magalhães, M.C. dos S. Nunes, E.M. Yoshimura, L.G. Jacobsohn, Thermoluminescence of UV-irradiated α-Al_2O_3:C,Mg, J. Lumin. (2020).

[10] N.M. Trindade, H. Kahn, E.M. Yoshimura, Thermoluminescence of natural $BeAl_2O_4$: Cr^{3+} Brazilian mineral: Preliminary studies, J. Lumin. 195 (2018) 356–361. https://doi.org/10.1016/j.jlumin.2017.11.057.

[11] N.M. Trindade, A.L.M.C. Malthez, A. de Castro Nascimento, R.S. da Silva, L.G. Jacobsohn, E.M. Yoshimura, Fabrication and characterization of a composite dosimeter based on natural alexandrite, Opt. Mater. (Amst). 85 (2018) 281–286. https://doi.org/10.1016/j.optmat.2018.08.066.

[12] A.M.B. Silva, D.O. Junot, L.V.E. Caldas, D.N. Souza, Structural, optical and dosimetric characterization of $CaSO_4$:Tb, $CaSO_4$:Tb, Ag and $CaSO_4$:Tb,Ag(NP), J. Lumin. (2020) 117286. https://doi.org/10.1016/j.jlumin.2020.117286.

[13] L. Jacobsohn, A. L. Roy, C.L. McPherson, C. Kucera, L. Oliveira, E. Yukihara, J. Ballato, Rare earth-doped nanocrystalline MgF_2: Synthesis, luminescence and thermoluminescence, 35 (2013) 2461–2464. https://doi.org/10.1016/j.optmat.2013.06.045.

[14] J.M. Kalita, G. Wary, Thermoluminescence properties of minerals and their application, LAP LAMBERT Academic Publishing, Saarbrucken, Germany, 2016.

[15] T.K. Kim, J.J. Woo, H.S. Choe, H.S. Kang, H.K. Jang, C.N. Whang, Thermoluminescence from Ultraviolet Exposed $MgAl_2O_4$, Radiat. Prot. Dosimetry. 84 (1999) 297–300. https://doi.org/10.1093/oxfordjournals.rpd.a032743.

[16] E.M. Yoshimura, E.G. Yukihara, Optically stimulated luminescence of magnesium aluminate ($MgAl_2O_4$) spinel, Radiat. Meas. 41 (2006) 163–169. https://doi.org/https://doi.org/10.1016/j.radmeas.2005.09.001.

[17] I. Ganesh, A review on magnesium aluminate ($MgAl_2O_4$) spinel: synthesis, processing and applications, Int. Mater. Rev. 58 (2013) 63–112. https://doi.org/10.1179/1743280412y.0000000001.

[18] V.T. Gritsyna, Y.G. Kazarinov, V.A. Kobyakov, I.E. Reimanis, Radiation-induced luminescence in magnesium aluminate spinel crystals and ceramics, Nucl. Instruments Methods Phys. Res. Sect. B Beam Interact. with Mater. Atoms. 250 (2006) 342–348. https://doi.org/10.1016/j.nimb.2006.04.135.

[19] V.T. Gritsyna, I. V Afanasyev-Charkin, V.A. Kobyakov, K.E. Sickafus, Structure and Electronic States of Defects in Spinel of Different Compositions $MgO{\cdot}nAl_2O_3$:Me, J. Am. Ceram. Soc. 82 (1999) 3365–3373. https://doi.org/10.1111/j.1151-2916.1999.tb02252.x.

[20] A. Lorincz, M. Puma, F.J. James, J.H.C. Jr., Thermally stimulated processes involving defects in γ- and x-irradiated spinel ($MgAl_2O_4$), J. Appl. Phys. 53 (1982) 927–932. https://doi.org/10.1063/1.330562.

[21] N. Kumamoto, T. Kato, N. Kawano, G. Okada, N. Kawaguchi, T. Yanagida, Scintillation and dosimeter properties of Ca-doped MgO transparent ceramics, Nucl. Instruments Methods Phys. Res. Sect. B Beam Interact. with Mater. Atoms. 435 (2018) 313–317. https://doi.org/10.1016/j.nimb.2018.01.023.

[22] A. Ibarra, M.J. de Castro, Thermoluminescence in $MgAl_2O_4$ X-ray irradiated at 90 K, J. Phys. Chem. Solids. 53 (1992) 1191–1198. https://doi.org/https://doi.org/10.1016/0022-3697(92)90038-F.

[23] J.F.S. Bitencourt, S.H. Tatumi, Synthesis and thermoluminescence properties of Mg^{2+} doped nanostructured aluminium oxide, Phys. Procedia. 2 (2009) 501–514. https://doi.org/https://doi.org/10.1016/j.phpro.2009.07.036.

[24] A. Ibarra, F. Mariani, R. Serna, J. Molla, M.J. De Castro, Thermoluminescence in $MgAl_2O_4$ above 300K, Radiat. Eff. Defects Solids. 119–121 (1991) 63–68. https://doi.org/10.1080/10420159108224855.

[25] Y. Takebuchi, H. Fukushima, D. Nakauchi, T. Kato, N. Kawaguchi, T. Yanagida, Scintillation and dosimetric properties of Ce-doped $MgAl_2O_4$ single crystals, J. Lumin. 223 (2020) 117139. https://doi.org/10.1016/j.jlumin.2020.117139.

[26] T. Kato, D. Nakauchi, N. Kawaguchi, T. Yanagida, Optical, scintillation, and dosimetric properties of dy-doped $MgAl_2O_4$ transparent ceramics, Optik (Stuttg). 207 (2020) 164433. https://doi.org/10.1016/j.ijleo.2020.164433.

[27] Y. Takebuchi, H. Fukushima, T. Kato, D. Nakauchi, N. Kawaguchi, T. Yanagida, Optical, scintillation, and dosimetric properties of Mn-doped $MgAl_2O_4$ single crystals, J. Mater. Sci. Mater. Electron. 31 (2020) 8240–8247. https://doi.org/10.1007/s10854-020-03359-x.

[28] M.S. Silva, S.T. Souza, D.V. Sampaio, J.C.A. Santos, E.J.S. Fonseca, R.S. Silva, Conductive atomic force microscopy characterization of PTCR-$BaTiO_3$ laser-sintered ceramics, J. Eur. Ceram. Soc. 36 (2016) 1385–1389. https://doi.org/10.1016/J.JEURCERAMSOC.2016.01.012.

[29] D.V. Sampaio, N.R.S. Souza, J.C.A. Santos, D.C. Silva, E.J.S. Fonseca, C. Kucera, B. Faugas, J. Ballato, R.S. Silva, Translucent and persistent luminescent $SrAl_2O_4:Eu^{2+}Dy^{3+}$ ceramics, Ceram. Int. 42 (2016) 4306–4312. https://doi.org/10.1016/J.CERAMINT.2015.11.108.

[30] J.C.A. Santos, E.P. Silva, D.V. Sampaio, N.R.S. Souza, Y.G.S. Alves, R.S. Silva, Radioluminescence emission of YAG:RE laser-sintered ceramics, Mater. Lett. 160 (2015) 456–458. https://doi.org/10.1016/J.MATLET.2015.08.017.

[31] N.R.S. Souza, D.C. Silva, D.V. Sampaio, M.V.S. Rezende, C. Kucera, A.A. Trofimov, L.G. Jacobsohn, J. Ballato, R.S. Silva, Laser sintering of persistent luminescent $CaAl_2O_4:Eu^{2+}Dy^{3+}$ ceramics, Opt. Mater. (Amst). 68 (2017) 2–6. https://doi.org/10.1016/J.OPTMAT.2016.10.050.

[32] Y.G.S. Alves, D.V. Sampaio, N.R.S. Souza, D.C. Silva, T.R. Cunha, C.T. Meneses, E.J.S. Fonseca, R.S. Silva, Persistent luminescence properties of $SrBXAl_2{-}XO_4$:Eu,Dy laser-sintered ceramics, Opt. Mater. (Amst). 70 (2017) 63–68. https://doi.org/10.1016/J.OPTMAT.2017.05.017.

[33] Z.S. Macedo, R.S. Silva, M.E.G. Valerio, A.L. Martinez, A.C. Hernandes, Laser-Sintered Bismuth Germanate Ceramics as Scintillator Devices, J. Am. Ceram. Soc. 87 (2004) 1076–1081. https://doi.org/10.1111/j.1551-2916.2004.01076.x.

[34] M. Okutomi, M. Kasamatsu, K. Tsukamoto, S. Shiratori, F. Uchiyama, Sintering of new oxide ceramics using a high power cw CO_2 laser, Appl. Phys. Lett. 44 (1984) 1132–1134. https://doi.org/10.1063/1.94666.

[35] Z.S. Macedo, R.S. da Silva, M.E.G. Valerio, A.C. Hernandes, Radiation detectors based on laser sintered $Bi_4Ge_3O_{12}$ ceramics, Nucl. Instruments Methods Phys. Res. Sect. B Beam Interact. with Mater. Atoms. 218 (2004) 153–157. https://doi.org/10.1016/j.nimb.2003.12.054.

[36] T.C. de Oliveira, M.S. da Silva, L.M. de Jesus, D.V. Sampaio, J.C.A. dos Santos, N.R. da S. Souza, R.S. da Silva, Laser sintering and radioluminescence emission of pure and doped Y_2O_3 ceramics, Ceram. Int. 40 (2014) 16209–16212. https://doi.org/10.1016/J.CERAMINT.2014.07.056.

[37] L.M. Jesus, J.C.A. Santos, D.V. Sampaio, L.B. Barbosa, R.S. Silva, J.-C. M'Peko,

Polymeric synthesis and conventional versus laser sintering of $CaCu_3Ti_4O_{12}$ electroceramics: (micro)structures, phase development and dielectric properties, J. Alloys Compd. 654 (2016) 482–490. https://doi.org/10.1016/j.jallcom.2015.09.027.

[38] L.M. Jesus, L.B. Barbosa, D.R. Ardila, R.S. Silva, J.-C. M'Peko, Effect of conventional and laser sintering on the (micro)structural and dielectric properties of $Bi_{2/3}Cu_3Ti_4O_{12}$ synthesized through a polymeric precursor route, J. Alloys Compd. 735 (2018) 2384–2394. https://doi.org/10.1016/j.jallcom.2017.10.140.

[39] A. Ibarra, D.F. Mariani, M. Jiménez de Castro, Thermoluminescent processes of $MgAl_2O_4$ irradiated at room temperature, Phys. Rev. B. 44 (1991) 12158–12165. https://doi.org/10.1103/PhysRevB.44.12158.

[40] C. Soliman, M.A. Hussein, Dysprosium oxide: A promising new thermoluminescent material for electron beam dosimetry, Radiat. Eff. Defects Solids. 159 (2004) 17–23. https://doi.org/10.1080/10420150310001635260.

[41] V. Pagonis, G. Kitis, C. Furetta, Numerical and Practical Exercises in Thermoluminescence, 1st ed., Springer-Verlag New York, 2006. https://doi.org/10.1007/0-387-30090-2.

[42] A. Halperin, A.A. Braner, Evaluation of Thermal Activation Energies from Glow Curves, Phys. Rev. 117 (1960) 408–415. https://doi.org/10.1103/PhysRev.117.408.

[43] R.K. Bull, Kinetics of the localised transition model for thermoluminescence, J. Phys. D. Appl. Phys. 22 (1989) 1375–1379. https://doi.org/10.1088/0022-3727/22/9/022.

[44] R. Chen, Glow Curves with General Order Kinetics, J. Electrochem. Soc. 116 (1969) 1254. https://doi.org/10.1149/1.2412291.

[45] R. Chen, On the Calculation of Activation Energies and Frequency Factors from Glow

Curves, J. Appl. Phys. 40 (1969) 570–585. https://doi.org/10.1063/1.1657437.

[46] C.M. Sunta, Unraveling Thermoluminescence, Springer India, 2015. https://doi.org/10.1007/978-81-322-1940-8.

[47] S.W.S. Mckeever, On the analysis of complex thermoluminescence. Glow-curves: Resolution into individual peaks, Phys. Status Solidi. 62 (1980) 331–340. https://doi.org/doi:10.1002/pssa.2210620139.

[48] G.F.J. Garlick, A.F. Gibson, The Electron Trap Mechanism of Luminescence in Sulphide and Silicate Phosphors, Proc. Phys. Soc. 60 (1948) 574. https://doi.org/https://doi.org/10.1088/0959-5309/60/6/308.

[49] H. Gobrecht, D. Hofmann, Spectroscopy of traps by fractional glow technique, J. Phys. Chem. Solids. 27 (1966) 509–522. https://doi.org/https://doi.org/10.1016/0022-3697(66)90194-6.

[50] R.S. da Silva, Z.S. Macedo, A.L. Martinez, A.C. Hernandes, M.E. Giroldo Valerio, Thermoluminescence kinetic parameters of $Bi_4Ge_3O_{12}$ single crystals, Nucl. Instruments Methods Phys. Res. Sect. B Beam Interact. with Mater. Atoms. 250 (2006) 390–395. https://doi.org/https://doi.org/10.1016/j.nimb.2006.04.144.

[51] J. Peng, Z. Dong, F. Han, tgcd: An R package for analyzing thermoluminescence glow curves, SoftwareX. 5 (2016) 112–120. https://doi.org/10.1016/j.softx.2016.06.001.

[52] V. Pagonis, S. Mian, G. Kitis, Fit of First Order Thermoluminescence Glow Peaks using the Weibull Distribution Function, Radiat. Prot. Dosimetry. 93 (2001) 11–17. https://doi.org/https://doi.org/10.1093/oxfordjournals.rpd.a006406.

[53] G. Kitis, J.M. Gomez-Ros, J.W.N. Tuyn, Thermoluminescence glow-curve deconvolution functions for first, second and general orders of kinetics, J. Phys. D. Appl. Phys. 31 (1998)

2636–2641. https://doi.org/https://doi.org/10.1088/0022-3727/31/19/037.

[54] A. Jun Peng aut, J. Burkardt ctb, J. More ctb, B. Garbow ctb, K. Hillstrom ctb, L.R. Petzold ctb, A.C. Hindmarsh ctb, R. Woodrow Setzer ctb, A. Horchler ctb, W. Cody ctb, C. Moler ctb, J. Dongarra ctb Maintainer Jun Peng, Package “tgcd” Type Package Title Thermoluminescence Glow Curve Deconvolution, (2019). https://doi.org/10.1007/BFb0067700.

[55] H.G. Balian, N.W. Eddy, Figure-of-merit (FOM), an improved criterion over the normalized chi-squared test for assessing goodness-of-fit of gamma-ray spectral peaks, Nucl. Instruments Methods. 145 (1977) 389–395. https://doi.org/10.1016/0029-554X(77)90437-2.

[56] R. Chen, S.A.A. Winer, Effects of Various Heating Rates on Glow Curves, J. Appl. Phys. 41 (1970) 5227–5232. https://doi.org/10.1063/1.1658652.

[57] M. Oberhofer, A. Scharmann, Applied thermoluminescence dosimetry, Bristol : Hilger, 1981. http://lib.ugent.be/catalog/rug01:000705616.

[58] A.M.B. Silva, D.O. Junot, L.V.E. Caldas, D.N. Souza, Structural, optical and dosimetric characterization of CaSO4:Tb, CaSO4:Tb, Ag and CaSO4:Tb,Ag(NP), J. Lumin. (2020) 117286. https://doi.org/10.1016/j.jlumin.2020.117286.